

## WATER AND DUST EMISSION FROM W HYDRAE

VICTOR ZUBKO<sup>1</sup> AND MOSHE ELITZUR

Department of Physics and Astronomy, University of Kentucky, Lexington, KY 40506-0055; zubko@pa.uky.edu, moshe@pa.uky.edu

*Received 2000 August 9; accepted 2000 September 25; published 2000 November 9*

### ABSTRACT

We construct a self-consistent model for the wind around W Hydrae by solving the coupled equations describing the hydrodynamics and dust radiative transfer problems. The model matches simultaneously the observed continuum radiation and wind velocity profile. The water line emission is calculated next using the water abundance as the only free parameter, fitted from the *Infrared Space Observatory* observations of Neufeld et al. and Barlow et al. The gas temperature is determined from a thermal balance calculation that includes water as one of its main components. Our model successfully fits all the observed water lines, resolving a major discrepancy between the modeling results of the two observing teams. The mass-loss rate is  $2.3 \times 10^{-6} M_{\odot} \text{ yr}^{-1}$ , the water abundance is  $1.0 \times 10^{-4}$ , and the ortho-to-para ratio is 1 : 1.3.

*Subject headings:* circumstellar matter — dust, extinction — infrared: stars — molecular processes — stars: AGB and post-AGB — stars: individual (W Hydrae)

### 1. INTRODUCTION

Water is a dominant coolant of outflows around cool oxygen-rich stars (Goldreich & Scoville 1976, Chen & Neufeld 1995, and Truong-Bach et al. 1999, hereafter GS, CN, and TB, respectively). However, until recently, observations of water cooling lines were impossible because of the atmospheric opacity at these wavelengths. The situation has changed with the successful launch of the *Infrared Space Observatory* (ISO). One of the first objects observed with ISO was W Hydrae, an M7.5 semiregular red giant, and it showed the expected thermal water emission in observations with both the short-wavelength spectrometer (SWS; Neufeld et al. 1996, hereafter N96) and long-wavelength spectrometer (LWS; Barlow et al. 1996, hereafter B96). Both teams also fitted their observations based on the GS approach, resulting in strikingly different estimates for the mass-loss rate:  $6 \times 10^{-7} M_{\odot} \text{ yr}^{-1}$  (B96) and  $(0.5\text{--}3) \times 10^{-5} M_{\odot} \text{ yr}^{-1}$  (N96). Here we aim to resolve this discrepancy. In contrast with the original studies, we construct a self-consistent model of the radiation field, dust, and gas in the shell, taking account of all the infrared continuum observations as an additional constraint.

### 2. MODELING

The driving force of the wind is radiation pressure on the dust; the gas particles are dragged along by collisions with the dust grains. The internal properties of the gas, such as temperature, do not play any role in the dynamics; the wind structure can be obtained by solving the coupled equations for hydrodynamics and dust radiative transfer. We now describe our calculation for W Hya. With the derived model we proceed to solve the H<sub>2</sub>O level population problem.

#### 2.1. Dynamics and IR Emission

A complete calculation of the wind structure requires a solution of the coupled hydrodynamics and dust radiative transfer problems. Traditionally these calculations involved a large number of input parameters. However, Ivezić & Elitzur (1995) noted that the dusty wind problem possesses general scaling properties such that, for a given type of grains, both the dy-

namics and radiative transfer depend primarily on a single parameter: the overall optical depth. Subsequent analysis by Ivezić & Elitzur (1997) established rigorously that the dust radiative transfer problem possesses scaling properties under the most general circumstances. Scaling was incorporated in the code DUSTY<sup>2</sup> (Ivezić, Nenkova, & Elitzur 1999), which solves fully the dusty wind problem. The solution provides the radial variation of the velocity and radiation fields in terms of the scaled distance  $y = r/R_{\text{in}}$ , where  $R_{\text{in}}$  is the shell inner boundary. That boundary is defined by the condition  $T_c = T_{\text{dust}}(y = 1)$ , where  $T_c$  is the dust condensation temperature. The actual value of  $R_{\text{in}}$  never enters.

We use for modeling “astronomical silicate” dust grains with optical constants from Laor & Draine (1993) and the power-law size distribution of Mathis, Rumble, & Nordsieck (1977). We assume prompt dust formation at  $y = 1$  and no further grain growth or destruction. The only input parameter in addition to the dust properties is the stellar temperature  $T_* = 2500$  K (Haniff, Scholz, & Tuthill 1995). From a series of DUSTY models in which we varied the visual optical depth  $\tau_v$ , the temperature  $T_c$ , and the shell outer radius  $Y = R_{\text{out}}/R_{\text{in}}$ , we chose the one that best fits all the observations all the way from  $1 \mu\text{m}$  to  $1.2 \text{ mm}$ ; because of its irregular variability, optical data is not included. We find that models with  $\tau_v = 0.7\text{--}1.0$ ,  $T_c = 900\text{--}1100$  K, and  $Y > 1000$  are almost equally successful in reproducing the observational spectrum. The most significant parameter by far is  $\tau_v$ ;  $T_c$  has only a small effect on the fitting, and the role of  $Y$  is marginal. The model with  $\tau_v = 0.83$ ,  $T_c = 1000$  K, and  $Y = 12,000$  minimizes the fitting errors and is presented in Figure 1. Matching the model flux to observations in scale as well as spectral shape determines the shell angular dimensions (Ivezić & Elitzur 1997). The shell inner diameter is  $0''.182$ , consistent with the measured stellar diameter  $0''.046$  (Haniff et al. 1995), and its outer diameter is  $36'$ , in agreement with the *IRAS* observations of Hawkins (1990).

#### 2.2. Water Lines

The statistical rate equations for the water level populations require the following input: the radiation field, to determine ra-

<sup>1</sup> On leave from the Main Astronomical Observatory, National Academy of Sciences, Kiev, Ukraine.

<sup>2</sup> Accessible at <http://www.pa.uky.edu/~moshe/dusty>.

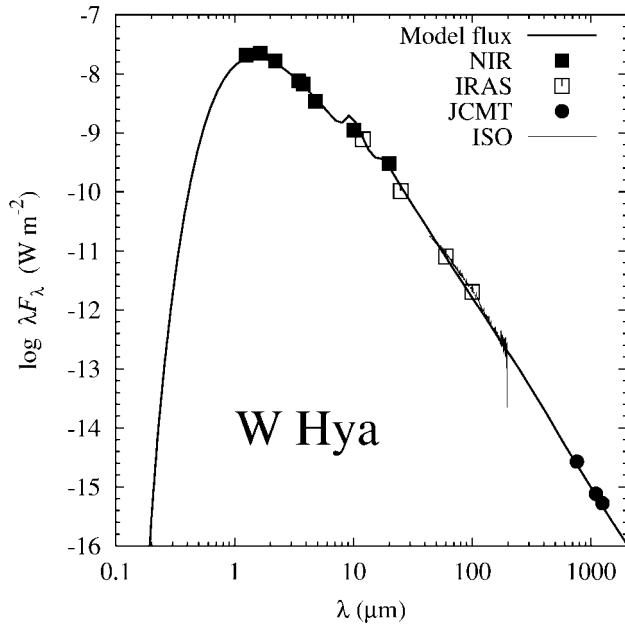


FIG. 1.—Spectral energy distribution of W Hya. Data indicated by filled squares (near-IR) are from Wilson et al. (1972), open squares (IRAS) are from Hawkins (1990), and filled circles (James Clerk Maxwell Telescope) are from van der Veen et al. (1995) and Walmsley et al. (1991). The thin solid line shows the ISO data of B96. The thick solid line is our model result.

diative excitations; the gas density and temperature, for the collision rates; and the water column density, required for the line radiative transfer (Elitzur 1992). DUSTY's output provides the radiation field as well as the dimensionless velocity and density profiles in the shell. Fixing the scale of densities requires two additional input properties. We take the distance  $d = 115$  pc from the *Hipparcos* catalog. This sets  $R_{\text{in}} = 1.6 \times 10^{14}$  cm and  $R_{\text{out}} \sim 1$  pc, and the luminosity is  $11,050 L_{\odot}$ , in agreement with Haniff et al. (1995). Next, the wind terminal velocity  $v_e = 8 \text{ km s}^{-1}$  (Young 1995) fixes the velocity scale and determines the gas-to-dust mass ratio  $r_{\text{gd}} = 850$  and the mass-loss rate  $\dot{M} = 2.3 \times 10^{-6} M_{\odot} \text{ yr}^{-1}$ . The complete velocity profile is shown in Figure 2 together with the data for OH and  $\text{H}_2\text{O}$  masers as well as CO thermal emission. All are properly explained by the model results. The SiO data is displaced from the wind velocity profile, as expected for this maser's location inside the dust formation zone (see Elitzur 1992).

The only required input quantities that remain unknown are the gas temperature and water abundance, and we fit those simultaneously from the water line observations. We calculate the temperature from the balance of cooling and heating due to adiabatic expansion, grain-gas collisions, and  $\text{H}_2\text{O}$  rovibrational transitions (we estimate the  $\text{H}_2$  vibrational contribution and find it negligible). We solve for the populations of the lowest 45 rotational levels of the ground vibrational state of ortho- and para-water; this accounts for all levels with energy  $\leq 2000$  K above ground. The molecular data are from the HITRAN database (Rothman et al. 1998), and the collision rate coefficients are from Green, Maluendes, & McLean (1993). The level populations and line emissivities are calculated with the escape probability method as functions of distance  $r$ , and the line fluxes by integrating the line emissivities over the shell volume. The free parameters are the abundances of the two water species, which must be considered independently since there is no radiative coupling between them. Detailed modeling

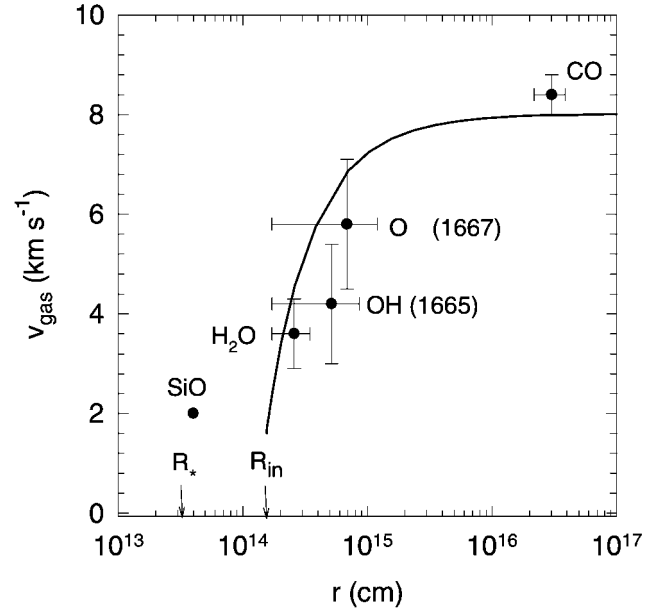


FIG. 2.—Model prediction for the gas velocity profile. Data points (from Szymczak, Cohen, & Richards 1998) show the  $\text{H}_2\text{O}$  and OH maser and CO thermal emission from the wind. The SiO maser emission originates in the extended atmosphere.

shows that these abundances are constant in the region where the water emission originates (CN, TB). Because of the central role of  $\text{H}_2\text{O}$  in the energy balance, the calculations of the temperature and water line emission are coupled and repeated until the best fit is achieved for the line observations. The best fit is found for water abundance  $n(\text{H}_2\text{O})/n(\text{H}_2) = 1.0 \times 10^{-4}$  and the ortho-to-para ratio of 1 : 1.3. Figure 3 shows the temperature profile. The model parameters are summarized in Table 1, and results and comparison with observations are shown in Table 2.

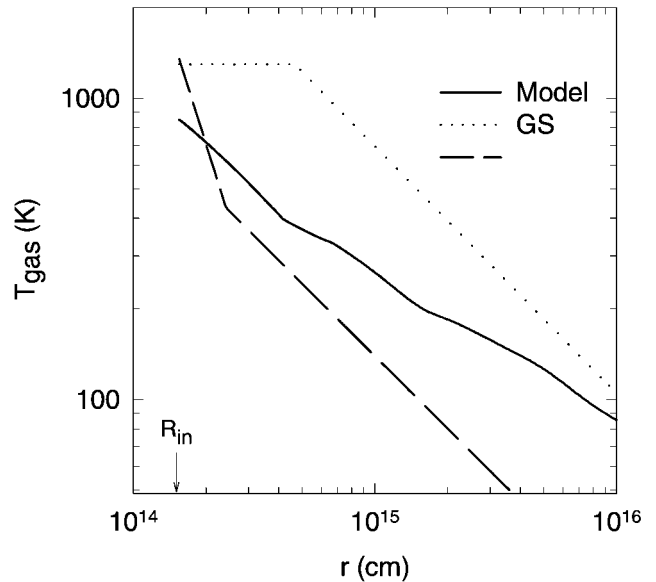


FIG. 3.—Gas temperature profile from our best-fit model. Shown are also power-law fits for the GS and CN temperature profiles.

TABLE 1  
MODEL PARAMETERS

Parameter	Value
Input:	
Stellar temperature <sup>a</sup> .....	2500 K
Distance <sup>b</sup> .....	115 pc
Final velocity <sup>c</sup> .....	8 km s <sup>-1</sup>
Fitting:	
Optical depth at 0.55 $\mu\text{m}$ <sup>d</sup> .....	0.83
Dust temperature at $R_{\text{in}}$ <sup>d</sup> .....	1000 K
Shell thickness ( $R_{\text{out}}/R_{\text{in}}$ ) <sup>d</sup> .....	12,000
H <sub>2</sub> O abundance at $R_{\text{in}}$ <sup>e</sup> .....	$1.0 \times 10^{-4}$
Ortho-H <sub>2</sub> O : para-H <sub>2</sub> O <sup>e</sup> .....	1 : 1.3
Derived:	
Stellar radius .....	$3.9 \times 10^{13}$ cm
Stellar luminosity .....	11,050 $L_{\odot}$
Shell inner radius ( $R_{\text{in}}$ ) .....	$1.6 \times 10^{14}$ cm
Mass-loss rate .....	$2.3 \times 10^{-6} M_{\odot} \text{ yr}^{-1}$
Gas-to-dust mass ratio .....	850
Shell outer radius ( $R_{\text{out}}$ ) .....	1.2 pc
Dust temperature at $R_{\text{out}}$ .....	17 K

<sup>a</sup> Haniff et al. 1995.

<sup>b</sup> *Hipparcos* catalog.

<sup>c</sup> Young 1995.

<sup>d</sup> Fitted from IR observations.

<sup>e</sup> Fitted from H<sub>2</sub>O lines.

### 3. DISCUSSION

Our model fits all the water lines within the observational errors, which generally exceed 50%. The quality of the fit for the LWS data is comparable to that of the B96 model. For the SWS data, N96 present a range of models for each line, and our model fits that data set better than any single one of them. Therefore, our model resolves the conflict among the previous water line calculations, fitting all the data with a single value for the mass-loss rate. It is important to note that  $\dot{M}$  is determined by the infrared data and  $v_e$  and remains unchanged during the modeling of the water lines. We find that the acceptable range of  $\dot{M}$  is  $\sim(2-3) \times 10^{-6} M_{\odot} \text{ yr}^{-1}$ , with a nominal value of  $2.3 \times 10^{-6} M_{\odot} \text{ yr}^{-1}$ . Except for the high end of the N96 range, most estimates of  $\dot{M}$  are in agreement with ours within the errors (see N96 and references therein).

The source of the large discrepancy with N96 is not clear. Neufeld et al. suggest that the temperature profile could be the reason, but this does not seem to be the case. Our temperature profile is not that different from the CN profile, which was used in the N96 study, especially in the relevant range  $T \gtrsim 400$  K (Fig. 3). We compared the various contributions to heating and cooling with those listed by CN and Neufeld & Kaufman (1993) and find good agreement; the difference in resulting profiles can be attributed to the different parameters used in the two calculations (CN used  $\dot{M} = 3 \times 10^{-5} M_{\odot} \text{ yr}^{-1}$ ). The two profiles differ much more with the GS profile employed in the B96 model, which produced  $\dot{M}$  similar to ours. We suspect that a more important source of difference could be the radiation field, since radiative excitations play an important role in the water population distribution. A comparison is impossible since N96 do not give details of the radiation field they employed. A proper radiation field appears crucial for the water line calculations.

The uncertainty in fitted parameters depends on the particular observations that constrain them. We estimate that the acceptable range for  $r_{\text{gd}}$  is  $\sim 850 \pm 100$ . We experimented with both power-law and single-size ( $a = 0.1 \mu\text{m}$ ) grain distributions and found the differences negligible. The large uncertainties in the measured line fluxes translate into a large uncertainty in the abundances of the two species of water. Between the two, the

TABLE 2  
OBSERVED AND MODEL FLUXES OF H<sub>2</sub>O LINES

$\lambda$ ( $\mu\text{m}$ )	Transition	$F_{\text{mod}}^a$	$F_{\text{obs}}^a$	$F_{\text{mod}}/F_{\text{obs}}$
180.486 .....	o: $2_{21} \rightarrow 2_{12}$	3.43	2.90	1.18
179.527 .....	o: $2_{12} \rightarrow 1_{01}$	12.48	8.66	1.44
174.624 .....	o: $3_{03} \rightarrow 2_{12}$	8.31	9.21	0.90
156.265 .....	o: $5_{23} \rightarrow 4_{32}$	2.42	5.41	0.45
144.517 .....	p: $4_{13} \rightarrow 3_{22}$	5.57	6.38	0.87
132.408 .....	o: $4_{23} \rightarrow 4_{14}$	2.97	5.50	0.54
125.356 .....	p: $4_{04} \rightarrow 3_{13}$	12.39	16.60	0.75
113.538 .....	o: $4_{14} \rightarrow 3_{03}$	11.27	17.40	0.65
108.073 .....	o: $2_{21} \rightarrow 1_{10}$	15.47	13.00	1.19
89.989 .....	p: $3_{22} \rightarrow 2_{11}$	18.11	27.30	0.66
83.283 .....	p: $6_{06} \rightarrow 5_{15}$	14.42	22.60	0.64
78.742 .....	o: $4_{23} \rightarrow 3_{12}$	14.08	28.00	0.50
67.089 .....	p: $3_{31} \rightarrow 2_{20}$	17.80	59.80	0.30
66.438 .....	o: $3_{30} \rightarrow 2_{21}$	18.45	22.90	0.81
63.458 .....	p: $8_{08} \rightarrow 7_{17}$	12.99	30.40	0.43
58.699 .....	o: $4_{32} \rightarrow 3_{21}$	15.35	19.50	0.79
57.637 .....	p: $4_{22} \rightarrow 3_{13}$	30.13	36.20	0.83
40.691 .....	o: $4_{32} \rightarrow 3_{03}$	36.07	23.00	1.57
31.772 .....	o: $4_{41} \rightarrow 3_{12}$	39.95	63.00	0.63
29.837 .....	o: $7_{25} \rightarrow 6_{16}$	30.72	32.00	0.96
37.984 .....	o: $4_{41} \rightarrow 4_{14}$	13.19	28.00	0.47 <sup>b</sup>

NOTE—Ortho transitions are marked by “o,” para transitions by “p.” The 57–180  $\mu\text{m}$  lines are from B96, and the 29–41  $\mu\text{m}$  lines are from N96.

<sup>a</sup> Fluxes are in units of  $10^{-20} \text{ W cm}^{-2}$ .

<sup>b</sup> This line is severely contaminated by blending with two others.

para-H<sub>2</sub>O abundance is subject to the larger uncertainty and can vary by as much as factor 3, so that the ortho-to-para ratio can be anywhere from 1 to  $\frac{1}{3}$ . By comparison, B96 obtained 1 for this ratio. All of these results differ greatly from the thermodynamic limit of 3. Depending on the ortho-to-para ratio, we find acceptable models for  $n(\text{H}_2\text{O})/n(\text{H}_2)$  in the range  $\sim(1-4) \times 10^{-4}$ .

In the modeling efforts of both B96 and N96,  $\dot{M}$  was one of numerous free parameters fitted from the water line observations. The scaling approach taken here reduces the number of free parameters to the essential minimum and determines  $\dot{M}$  prior to the water line fitting. Table 1 breaks the model parameters into three categories. Quantities in the first division are specified as input, in addition to the IR and water observations. The second group includes the free parameters of our two fitting procedures, while the third group lists results derived from our fits. Given grain properties, the IR observations are fitted with the three free parameters— $\tau_v$ ,  $T_c$ , and  $Y$ —and the single independent input  $T_*$ . The resulting model determines also the dimensionless velocity profile. Adding as independent input the source distance and the wind final velocity, the model results determine the full velocity profile, and  $\tau_v$  determines also  $\dot{M}$  and the gas-to-dust ratio. Fitting the water lines involves no other input and only two free parameters—the ortho- and para-water abundances. Thanks to the central role of water lines in the gas temperature calculation, the gas temperature is determined self-consistently as part of this second fitting procedure. Since the only free parameters in fitting the observed water fluxes are the abundances of the two species, confidence in the derived values is greatly enhanced. In principle, we could have used  $\dot{M}$  as a free parameter in the water calculations, as in the previous studies. In that case, consistency between the results of the two fitting procedures would be used as an additional constraint, automatically met by our calculation.

While radiation pressure on the dust grains is generally ac-

cepted as the driving mechanism behind the wind expansion, this mechanism has not been fully tested. The solutions of radiative transfer and the hydrodynamics problems must result in the same parameters, but this fundamental test has not been performed thus far; self-consistent modeling of both the IR emission and the wind structure in the same source has not yet been attempted. The most detailed previous calculation we are aware of is the TB modeling of R Cas. However, in that work the radiation field was not calculated self-consistently; instead it was derived from a dust temperature profile that was assumed beforehand as an input property. In contrast, DUSTY determines this temperature from a proper calculation of radiative equilibrium coupled to the radiative transfer including dust scattering, absorption, and emission. The spectral energy distribution is fitted with just three free parameters, only one of which ( $\tau_v$ ) is significant. Once these parameters are set, the

outflow terminal velocity determines the entire velocity profile without any more freedom in the model. It is highly significant that a single self-consistent model with the minimal necessary number of parameters provides agreement with both the spectral energy distribution and the molecular velocity observations. Apart from resolving the  $\dot{M}$  discrepancy in W Hya, the success of our model provides strong support for the basic paradigm of winds in late-type stars.

We thank Michael Barlow for the *ISO* LWS spectrum of W Hya, David Neufeld for help with the water molecular data, Željko Ivezić for his comments on the manuscript, and the referee for useful suggestions and for pointing out the *Hipparcos* distance measurement. The partial support of NASA and NSF is gratefully acknowledged.

#### REFERENCES

- Barlow, M. J., et al. 1996, *A&A*, 315, L241 (B96)  
 Chen, W., & Neufeld, D. A. 1995, *ApJ*, 453, L99 (CN)  
 Elitzur, M. 1992, *Astronomical Masers* (Dordrecht: Kluwer)  
 Goldreich, P., & Scoville, N. 1976, *ApJ*, 205, 144 (GS)  
 Green, S., Maluendes, S., & McLean, A. D. 1993, *ApJS*, 85, 181  
 Haniff, C. A., Scholz, M., & Tuthill, P. G. 1995, *MNRAS*, 276, 640  
 Hawkins, G. W. 1990, *A&A*, 229, L5  
 Ivezić, Ž., & Elitzur, M. 1995, *ApJ*, 445, 415  
 ———. 1997, *MNRAS*, 287, 799  
 Ivezić, Ž., Nenkova, M., & Elitzur, M. 1999, User Manual for DUSTY, Univ. Kentucky Internal Rep.  
 Laor, A., & Draine, B. T. 1993, *ApJ*, 402, 441  
 Mathis, J. S., Rumble, W., & Nordsieck, K. H. 1977, *ApJ*, 217, 425  
 Neufeld, D. A., & Kaufman, M. J. 1993, *ApJ*, 418, 263  
 Neufeld, D. A., et al. 1996, *A&A*, 315, L237 (N96)  
 Rothman, L. S., et al. 1998, *J. Quant. Spectrosc. Radiat. Transfer*, 60, 665  
 Szymczak, M., Cohen, R. J., & Richards, A. M. S. 1998, *MNRAS*, 297, 1151  
 Truong-Bach, et al. 1999, *A&A*, 345, 925 (TB)  
 van der Veen, W. E. C. J., Omont, A., Habing, H. J., & Matthews, H. E. 1995, *A&A*, 295, 445  
 Walmsley, C. M., Chini, R., Steppe, H., Forveille, T., & Omont, A. 1991, *A&A*, 248, 555  
 Wilson, W. J., Schwatz, P. R., Neugebauer, G., Harvey, P. M., & Becklin, E. E. 1972, *ApJ*, 177, 523  
 Young, K. 1995, *ApJ*, 445, 872